The role of Laplace pressure in the maximal weight of pendant drops

Laure Lecacheux, Abdelkrim Sadoudi, Agnès Duri-Bechemilh, Véronique Planchot, Thierry Ruiz

The role of Laplace pressure in the maximal weight of pendant drops

Laure Lecacheux[1,2], Abdelkrim Sadoudi[2], Agnès Duri[2], Véronique Planchot[2], Thierry Ruiz[1*]

[1] UMR QualiSud, Univ. Montpellier, CIRAD, Montpellier SupAgro, Univ. Avignon, Univ. La Réunion – 15 avenue Charles Flahault, 34093, Montpellier cedex 5, France.

[2] UMR IATE 1208 INRAE/Montpellier SupAgro/Univ. Montpellier – 2 Place Pierre Viala, 34060 Montpellier cedex 1, France.

[*] corresponding author

Email. thierry.ruiz@umontpellier.fr

Abstract.

Hypothesis

The value of the maximal weight of a pendant drop formed at the end of a syringe needle is lower than the intensity of the corresponding capillary force. The balance of the external forces applied to the maximal pendant drop must be completed by the overpressure generated by the piston of the syringe. Inside the drop, the Laplace pressure corresponds to this overpressure.

Experiments

Pendant drops are made with three liquids and five different needle diameters. The influence of Laplace pressure on the maximal weight is experimentally highlighted by modulating the

drop curvatures thanks to glass beads placed at the apex of the pendant drop. Their maximal weight and curvatures are measured by image analysis.

Findings

Experiments confirm that the balance of external forces must be completed by the force acting on the syringe piston. The overpressure on the piston has an impact on the drops via the Laplace pressure. A master curve between the mean curvature and the maximal volume of the pendant drops is observed. This result allows to validate an expression of the maximal weight which integrates the Laplace pressure. This work contributes to a better understanding of the maximal pendant drop properties and beyond, of the capillary phenomenon.

Keywords. Pendant drop; Maximal drop weight; Capillary force; Laplace pressure; Curvature; Image analysis.

Nomenclature

Abbreviations

b	(glass) bead
d	drop
e	external
eq	equilibrium
i	internal
l	liquid
n	needle

p	piston
*	loaded drop

Symbols

B_o	Bond number [-]
$2H$	mean curvature [m^{-1}]
D_n	Diameter of the needle [m]
$\vec{F}_p$	force increment applied by the piston on the pendant drop [N]
$\vec{F}_c$	capillary force at the wetted perimeter [N]
g	gravity acceleration [$m.s^{-2}$]
H_l	height of liquid colum in the syringe [m]
L_n	needle length [m]
M_b	mass of a glass bead [kg]
M_d	maximal mass of a pendant drop [kg]
M_d^*	maximal mass of a loaded pendant drop [kg]
M_l^*	mass of the liquid in a loaded pendant drop [kg]
P_n	pressure at the end of the needle [Pa]
P_p	pressures at the piston [Pa]
Q	feeding volume flow rate [$m^3.s^{-1}$]
R_e	Reynolds number [-]
R_1	radial curvature radius [m]
R_2	axial curvature radius [m]
$\vec{v}_d$	barycentric velocity of the drop [$m.s^{-1}$]
V_d	maximal volume of a single pendant drop [m^3]

V_d^* maximal volume of a loaded pendant drop [m^3]

$\vec{z}$ vertical position from the bottom of the needle [m]

γ surface tension of the liquid [$N.m^{-1}$]

ΔP_L Laplace pressure [Pa]

ΔP_n overpressure within the fluid at the end of the needle [Pa]

ΔP_p overpressure at the piston [Pa]

$\Delta P_{p\to n}$ pressure drop in the syringe [Pa]

Δz incremental displacement of the piston lowering [Pa]

η viscosity of the liquid [Pa.s]

θ wetting angle [rad]

κ^{-1} capillary length [m]

ρ_l true density of the liquid [$kg.m^{-3}$]

ρ_b true density of the glass [$kg.m^{-3}$]

Ω_s internal section of the syringe [m^2]

1. Introduction

Pendant drops at the end of a syringe capillary, are easily made objects that have a regularity of size and shape, offering the possibility to use them in multiple applications. They can be used as micromanipulators to capture small objects by capillary interaction thanks to the formation of a liquid-bridge at their apex [1,2]. These same capillary interactions are also used to structure assemblies of colloidal or granular particles. Liquid marbles are other applications that implement these surface interactions with colloids [3,4,5]. Drops are also used for agglomeration or granulation unit operations [6,7]. The drop properties (in particular their size and volume), which interact with powder to associate them into agglomerated

structures [8,9], require a precise control in order to best master the associative processes [10,11]. Because the small drop volume is circumscribed by surface tension, it can also be directly used as a millireactor where various chemical reactions can be performed [12,13]. The pendant drop of a colloidal suspension or a macromolecular solution constitutes a reactional volume in which a "stoichiometric forcing" can occur as the volume decreases by evaporation [14]. In spray-drying, specific reactions are achievable and the control of the structural mechanisms to which they lead, requires the mastering of the evolution of the drop volume which can be studied in a pendant configuration [15]. Pendant drops are also employed to determine the surface tension of a liquid [16,17,18], from the analysis of the shape of a pendant drop in equilibrium and matching its contouring curve to a mathematical solution of the Young-Laplace equation. This inverse method allows to identify the surface tension value which represents the fitting factor.

There is a second method, called the drop weight method [19], which is based on the comparison between the weight of a falling drop (measured) and its theoretical value estimated from Tate's law [20]. The surface tension is the adjustment parameter that allows to fit these two values. Tate's law relates the maximum weight of a pendant drop to the capillary force that holds the drop in equilibrium at the end of a syringe needle, just before it falls off. Since only part of the pendant drop falls off, leaving a residual fraction on the needle, it is necessary to correct the weight of an "ideal drop" given by Tate's law by a correction factor. Among the most widely used works for this purpose, that of Harkins and Brown [21] proposes values of the correction factor tabulated on a chart. But the exact calculation of the maximum weight just before its detachment would ensure even greater precision.

The aim of this work is to determine the maximal weight of a pendant drop at the end of a syringe needle by experimental investigations and theorical developments. We propose to

125 define a consistent expression of the maximum weight of a pendant drop. No particular
126 application of this result will be favored. Experimental results related to the measurement of
127 the maximal weight of drops performed with three liquids of different known surface tensions
128 and five different needle sizes, are presented. These experiments are carried out at small Bond
129 numbers of the needle in order to achieve the same drop shape (piriform). We observe that the
130 weight of the pendant drop is not equal to the capillary force which ensures the drop/needle
131 connection. This gap is attributed to the lack of a force in the balance of external forces
132 applied to the drop. In order to reveal the importance of this missing force, mechanical stress
133 tests are performed by adding a calibrated glass bead at the apex of the drop, without
134 changing the intensity of the capillary force. Beads of increasing mass induce a variation of
135 the mean curvature directly associated with a variation of the maximal weight of the drops
136 following a master curve. The repercussion of these variations on the Laplace pressure
137 generates a force which completes the force balance. To demonstrate mathematically this
138 important point, a physical reasoning, based on the fluid mechanics, is developed. These
139 results allow us to introduce the Laplace pressure in the mathematical model which predicts
140 the maximal weight of a pendant drop.
141
142 **2. Experimental procedure**
143
144 **2.1. Prototype description**
145
146 A prototype, presented in Figure 1, was designed to study the formation of a pendant drop at
147 the end of a capillary until its maximal volume, just before its detachment. It consists of a PPT
148 syringe composed of a body of an internal section $\Omega_S = 61$ mm^2, a piston and a tapered tip
149 allowing the adaptation of a straight cut steel needle (Doseurope) of section Ω_{ni}. Five

150 different needle sizes were used. Their external diameter D_{ne} is: 0.23, 0.5, 0.8, 1.26 and 1.80
151 mm and their internal diameter D_{ni} is respectively: 0.11, 0.26, 0.51, 0.84 and 1.37 mm. In
152 order to ensure a constant flow rate of liquid ($Q \sim 0.097$ to 0.387 $mm^3.s^{-1}$), a syringe pump
153 driven by a stepper motor (MicroLYNX, M-1410-0.75D) is used to provide a vertical
154 displacement according to $\vec{z}$. This flow rate gives a velocity intensity in the needle comprised
155 between 0.26 and 5 $mm.s^{-1}$. For each test, the laminar flow inside the needle is achieved with
156 a Reynolds number comprised between 18×10^{-3} (Triacetin with the largest needle) and
157 5.6×10^{-1} (water with the smallest needle). The evolution of the pendant drop formation until
158 its maximal volume is filmed using a USB microscope (DinoLite®) placed in front of the
159 needle with an acquisition rate of 25 $images.sec^{-1}$. A LED backlight system is also used to
160 enhance the contrast.
161
162 The prototype is placed on an insulated support to avoid any vibration and is isolated in a
163 plexiglass chamber to minimize any contamination. All the tests are performed in quintuples,
164 at a controlled temperature of 25.0 ± 0.2 °C, and a relative humidity of 40 ± 16 %. The total
165 duration of formation of a drop is between 1 and 2 minutes which allows to neglect the
166 evaporation phenomena [22].
167
168 **2.2. Characteristics of liquids**
169
170 Pure water, Tween® 80 (Sigma-Aldrich) diluted at 2×10^{-3}g/L, and Triacetin® (C2 99.0%,
171 Sigma-Aldrich) are the three considered liquids. The surface tension, γ, measured using a
172 tensiometer Kruss K100 (Kruss, Germany) according to the Wilhelmy plate, is equal to
173 71.83±0.59 $mN.m^{-1}$ for water, 43.74±0.09 $mN.m^{-1}$ for Tween 80, and 34.55±0.25 $mN.m^{-1}$ for
174 Triacetin. The density, ρ_l, obtained thanks to DSA 5000M sonodensimeter (Anton Paar,

175 France), corresponds to 0.997±0.001 g.cm^{-3} for water and Tween 80, and 1.152±0.001 g.cm^{-3}
176 for Triacetin. The viscosity, η, determined using a rheometer Physica MCR 301 equipped
177 with a double gap mobile (Anton Paar, Austria), has the value of 1.005±0.005 mPa.s for
178 water, 1.010±0.012 mPa.s for Tween 80, and 23.021±0.001 mPa.s for Triacetin. All
179 measurements were performed in triplicate at 25°C.
180
181 These three liquids are distinguished by the capillary length: $\kappa^{-1} = \sqrt{\gamma/\rho_l g}$, sufficiently
182 contrasted (2.71 mm for water, 2.11 mm for Tween 80 and 1.83 mm for Triacetin) to show
183 differences in the geometric characteristics of the drops. For each tested configuration, the
184 Bond number of the drop: $B_{od} = (R_1/\kappa^{-1})^2 < 1$ (Fig. 2) and the Bond number of the needle:
185 $B_{on} = (D_{ne}/2\kappa^{-1})^2 < B_{od}$, ensure a piriform geometry of the drops.
186
187 **2.3. Description of the mechanical test**
188
189 This mechanical test, adapted from the works of Li et al. [23] and Neeson et al. [24], consists
190 in loading with a calibrated particle of known mass a pendant drop obtained from a needle of
191 a given diameter. Then the maximal weight of the loaded drop just before its detachment is
192 measured. In order to highlight the role of Laplace pressure on the weight of a pendant drop,
193 this test allows to modulate the main curvatures of the drop (see video).
194
195 The aim of this test is to achieve conditions that ensure invariance of the capillary force at the
196 drop/needle wetted perimeter while modulating Laplace pressure within the drop. When the
197 drop reaches a stage of development corresponding to about 30% of its maximum volume, the
198 glass bead is then approached to its apex. At its contact, the drop exerts a capillary traction
199 that captures the bead and keeps it in suspension in a position that respects the global

200 axisymmetry (Fig. 2). The hydrodynamic flow conditions in the syringe allow a quasi-
201 stationary evolution of the growth of the loaded drop. The shape of the drop, and in particular
202 its main curvatures, adapt to the resultant external forces applied to it [24]. Six spherical glass
203 beads (density of 2.501 g.cm^{-3}) of different masses (0.62, 1.48, 2.55, 4.52, 8.38 and 12.03 mg)
204 are used. The Bond numbers of the glass beads are less than 1, which ensures their capillary
205 capture by the pendant drop.
206
207 The operating conditions are identical to those used during the formation of a single pendant
208 drop and the evolution of the loaded drops is also captured by the USB microscope (Fig. 1).
209
210 **2.4. Determination of drop characteristics**
211
212 An image analysis method was developed to determine the maximum pendant drop volume
213 and the two radii of curvature. Technical details are given in the Supplementary Materials file.
214
215 *Maximal volume.* Each drop is filmed (from 1 to 2 min at 25 fps) during its entire
216 development and all the images are extracted (from 1500 to 3000) then analyzed to precisely
217 determine the maximum volume of each pendant drop. The linear progression of the volume
218 of the drop, due to the constant flow, makes it possible to locate the maximal volume reached
219 with an error less than 0.01 %. The maximum weight is then calculated from the
220 determination of the volume.
221
222 *Radius of curvature, main curvature and Laplace pressure.* The image, corresponding to the
223 limit stage of drop development, is used to determine the curvature radii. The curvature radius
224 R_1, is determined at the level of the maximum diameter in the horizontal plane. The curvature

radius R_2, is located in the vertical plane, and corresponds to the radius of the circle being superimposed with the drop curve [18]. The main curvature of the drop is then deduced from these measurements according to its standard definition in 3D space, $2H = \frac{1}{R_1} + \frac{1}{R_2}$. The Laplace pressure in the drop is then calculated according to its definition [25]: $\Delta P_L = \gamma 2H$. This procedure is used for single and loaded drops.

3. Results and discussion

3.1. Maximal weight of a pendant drop

Pendant drops are formed at the end of needle of a syringe using a stationary flow rate of the liquid, Q, ensured by a force $\vec{F}_p$ applied on the piston. The maximal mass reached by the drop, M_d, is calculated from the measurement of the volume. The laminar regime ensures the stability of the drop formation and we verify that neither the value of the flow nor the height of liquid (H_l) between the surface of the piston and the lowest part of needle, does not change the maximal mass of the drop (see Supplementary Materials file). This point implies that the hydrostatic pressure does not affect the maximal weight of a pendant drop generated by a syringe.

In these conditions, the balance of the external forces applied to a pendant drop takes into account only three actions (the weight, the capillary force exerted at the triple line and inertia [25]), and can be written as follow:

$$M_d \vec{g} + \vec{F}_c = M_d \frac{d\vec{v}_d}{dt} \approx \vec{0} \quad (1)$$

where the inertial force is negligible when a steady state is imposed (a constant flow rate implies that the barycentric velocity of the drop inertia center, $\vec{v}_d$, remains constant). The projection of this vectorial equation on the horizontal axis cancels out, while on the vertical axis we find that the weight must be compensated by the projection of the capillary force on $\vec{z}$. Assuming that the intensity of the capillary force is equal to [25]: $F_c = \pi D_{ne} \gamma \cos(\theta)$, for each tested condition, the wetting angle θ at the drop connection on the outer perimeter of the needle is checked. It is always close to 0° and does not impact the value of the capillary force, as already observed by Nazari et al. [26]. With this definition, the maximal weight of the pendant drop is given by:

$$M_d g = \gamma \pi D_{ne} \quad (2)$$

This expression is well known as the Tate's law [20, 27], and the maximal weight defined by Equation (2) is classically called the weight of the "ideal drop". We remind that this maximum weight is the weight of a pendant drop still attached to its needle and not the weight of a detached drop. By plotting the measurements of the maximum drop weight as a function of the corresponding capillary force for each tested case, it can be clearly observed in Figure 3a that Equation (2) is not verified. The capillary force is systematically higher than the weight, and this gap is about 35.0% ±1.2% on average. Surprising as it may seem, we are not aware of any experimental data in the scientific literature on the weight of pendant drops. All the numerous works deal with detached drops with all the precautions on the validity of Tate's law. Lee et al. [28] pointed out that the force balance used to define the weight of the "ideal drop" does not include a compressive force in the upper plane of the drop. This balance needs to be redefined [29,30]. Therefore, such a gap implies to consider again the balance of external efforts applied to a pendant drop [30] taking into account the repercussion of the

force increment applied on the piston, $\vec{F}_p$, called the Laplace force, on the pendant drop. A drop generated by a syringe is only developed by the action of a force increment on the piston. This force is oriented in the same direction as the weight and is transmitted until the top surface of the drop: $\pi D_{ni}^2/4$, via an overpressure throughout the liquid column. We can show that this overpressure corresponds to the Laplace pressure in the pendant drop. The expression of the external force balance becomes:

$$M_d\vec{g} + \vec{F}_p + \vec{F}_c \approx \vec{0} \quad (3)$$

Under all these hypotheses and by introducing the definition of the Laplace pressure in the external force balance exerted on the pendant drop, Equation (3) can be written as:

$$M_d g = \gamma\pi D_{ne} - \Delta P_L \pi D_{ni}^2/4 \quad (4)$$

This equation involves the internal D_{ni}, and external D_{ne} diameters of the needle. From Laplace's pressure measurements, we verify in Figure 3b that the maximal weight of a pendant drop is then well described by Equation (3).

We propose in the following section an experiment at the drop level in order to highlight the role of the Laplace pressure and the trend with which it acts on the maximal weight drop. The implication of Laplace pressure in the balance of external forces applied to a pendant drop has already been suggested by Garandet et al. [29]. However, our approach highlights the non-contribution of hydrostatic pressure, contrary to the equation presented by Garandet et al. [29]. We also provide an explanation of the origin of this involved Laplace force and a justification by establishing a model under well-identified hypotheses.

3.2. Drop loading to highlight the Laplace pressure

The drop keeps held to the needle by the capillary force at its triple line which equilibrates the weight added to the force applied on the piston transmitted to the drop via the pressure in the liquid column. The test consists of keeping the capillary force constant (constant needle diameter and constant surface tension of the liquid) and varying the drop weight by distributing it between the liquid and a glass bead placed at the apex. Whatever its weight, the presence of a glass bead does not modify the intensity of the capillary force exerted on the pendant drop due to the fact that: (*i*) the wetted perimeter is unchanged, (*ii*) the contact angle value just before drop detachment has been systematically measured by image analysis (Fig. 4) and remains unchanged: $\theta \approx 0°$, and (*iii*) the liquid surface tension is not modified (the beads are carefully cleaned beforehand). Thus, the force balance (Eq. 4) is satisfied for the maximal total weight of the loaded drop: $M_d^* g = M_b g + M_l^* g$, where $M_l^* g$ is the liquid weight and $M_b g$ is the glass bead weight. The weight of the bead has an impact on the shape of the drop (Fig. 4) and therefore on the Laplace pressure inside the drop. The drop loading with a glass bead constitutes therefore a reliable mechanical test with a fixed capillary force.

For each liquid, increasing loads with calibrated glass beads were realised for all pendant drops obtained with the five needles. Figures 5 presents an illustration of the maximal weight of the loaded pendant drops, as a function of the bead mass. Whatever the needle diameter and the liquid, the maximal weight of the loaded drops is not constant but decreases with the increase of the bead mass. In all cases, $M_d g > M_d^* g$ and so, the hypothesis of the capillary force, only opposed to the weight of the maximal pendant drop in the external force balance, is invalidated by the imposed conditions in these experiments.

This result indicates that at constant capillary force, if the maximum weight of a pendant drop decreases with increasing loads, then the Laplace pressure should increase to ensure the external force balance (Eq. 4).

In order to determine the Laplace pressure in the drop, the mean curvature is measured. For a given needle, as the particle mass increases, a loaded drop adopts an increasingly elongated shape (Fig. 4). The axisymmetry being satisfied, the quantitative analysis of the main curvatures (Fig. 2) shows that the increasing mechanical solicitation induces an elongation of the axial radius of curvature (vertical plane), R_2, and simultaneously a narrowing of the radial radius of curvature (horizontal plane), R_1 (Fig. 6a). For each liquid and each needle, the radii of curvature of the loaded drops are resized by those of the unloaded drops made with the same needle: R_1^*/R_1 and R_2^*/R_2. The antagonistic variation of the two radii of curvature systematically leads to an increase of the mean curvature defined by: $2H^* = \frac{1}{R_1^*} + \frac{1}{R_2^*}$, for all loaded pendant drops.

Figure 6b shows that $2H^*/2H$ ratio increases linearly with the solid mass fraction and is superimposed on a single curve for all experiments.

For each tested liquid and needle, experiments show that loading induces a decrease of the maximal weight of the pendant drops (Fig. 5) and an increase of the Laplace pressure (Fig. 7). This point represents an experimental validation of the influence of the Laplace pressure in the weight of a pendant drop. The expression of the external force balance given by Equation (3) seems more correct than Equation (1).

Because of the glass and liquid incompressibility, the volumes of unloaded drops and loaded drops are respectively given by: $V_d = M_d/\rho_l$, and $V_d^* = M_l^*/\rho_l + M_b/\rho_b$. For all maximal drops (loaded and unloaded), a well-defined relationship is shown between the mean curvature and the volume of a maximal pendant drop (Fig. 8). This power law dependence between these geometrical quantities constitutes a master curve for the maximal pendant drops. When unloaded maximal pendant drops are quasi-spherical, which is the case for very small drops, $R_1 \approx R_2 \approx R$, the curvature follows a power law with the volume: $2H \sim V_d^{-\frac{1}{3}}$. Such a trend is experimentally obtained as shown in Figure 8a.

Regardless of the mechanical loading, for each liquid and according to the variation of the mean curvature, Laplace pressure decreases with the maximal weight of the pendant drops (Fig. 8b). The surface tension value discriminates Laplace pressure levels within drops made of different liquids. At equal density, the mixture of water and Tween 80 has a lower surface tension than water, so the Laplace pressure is lower.

3.3. Demonstration of maximal pendant drop weight expression

For a pendant drop generated at the end of a syringe needle, the external force balance (Eq. 3) includes (Fig. 9): (*i*) the weight of the drop: $M_d\vec{g}$, (*ii*) the force increment applied on the piston that propagates until the drop via the internal section of the needle ($\pi D_{ni}^2/4$): $\vec{F}_p$, and (*iii*) the capillary force at the wetted perimeter (here the outer perimeter of the needle): $\vec{F}_c$. The rigorous demonstration that the intensity of the force $\vec{F}_p$ is related to the Laplace pressure is not so obvious. The intensity F_p exerted on a pendant drop can be written as a function of the overpressure at the piston (ΔP_n) within the fluid at the end of the needle: $F_p = \Delta P_n \pi D_{ni}^2/4$

(the force exerted on the piston equals: $\Delta P_p \Omega_s$). The overpressure ΔP_n can be calculated from the momentum balance of the flowing fluid between the piston and the end of the needle. Assuming that the liquid is incompressible and the flow in a steady-state, Bernouilli's equation gives:

$$P_p + \rho_l g(H_l - \Delta z) + \frac{1}{2}\rho_l \frac{Q^2}{\Omega_s^2} = P_n + \frac{1}{2}\rho_l \frac{Q^2}{\Omega_{ni}^2} + \Delta P_{p\to n} \quad (5)$$

with Δz, the displacement corresponding to the piston lowering, P_p and P_n respectively the pressures in the liquid at the piston interface and at the end of the needle, and $\Delta P_{p\to n}$ the drop pressure between the piston and the end of the needle. During all the pendant drop formation, the ratio $\Delta z/H_l$ remains below 1 %. The term contributions related to the kinetic energy: $\frac{1}{2}\rho_l Q^2/\Omega_s^2$ and: $\frac{\frac{1}{2}\rho_l Q^2}{\Omega_{ni}^2}$, take values of the order of magnitude of 10^{-4} Pa at most and are therefore negligible. Due to the large gap between the internal sections of the syringe and the needle ($\Omega_{ni}/\Omega_s \approx 0.025$ at most), the pressure drop in the body of the syringe is negligible compared to the one in the needle. The flow occurs in laminar regime so, we assume that the pressure drop is given by Hagen-Poiseuille formula: $\Delta P_{p\to n} = \frac{128\eta L_n Q}{\pi D_{ni}^4}$, with η the viscosity of the liquid and L_n the length of the needle. With these value ranges of the parameters, this pressure drop does not exceed $\sim 10^2$ Pa in the worst case (Triacetin with the smallest needle) and ~ 10 Pa for all other conditions. Therefore, the viscous dissipation can be neglected compared to the other pressure values ($\sim 10^5$ Pa). Under these considerations, the balance (Eq. 5) can be reduced to the hydrostatic part:

$$P_n \approx P_p + \rho_l g H_l \quad (6)$$

As the liquid was initially drawn into the syringe by the application of a vacuum, the condition of hydrostatic equilibrium that precedes the application of the overpressure to the piston can be written as: $P_n^{eq} = P_p^{eq} + \rho_l g H_l$, where P_n^{eq} and P_p^{eq} are the pressures at equilibrium after the entrance of the liquid. When the pendant drop is generated, the overpressure applied to the piston is given by: $\Delta P_p = P_p - P_p^{eq}$, and is transmitted to the end of the needle by: $\Delta P_n = P_n - P_n^{eq}$. The momentum balance (Eq. 6) leads to the conclusion that $\Delta P_p \approx \Delta P_n$. In quasi-static conditions, the overpressure applied to the piston is transmitted to the drop. We find that hydrostatic pressure no longer plays a role on the drop weight, as experimentally verified (see Supplementary materials file).

For the studied configuration and the implemented process conditions, we verified that the stationary kinetics of the drop growth can be assimilated to a succession of equilibrium states ($1.8\times10^{-2} \leq R_e \leq 5.6\times10^{-1}$). Under this hypothesis of local quasi-static state, we consider that the expression of the overpressure within the drop can be given by the Laplace-Young relation. Consequently, $\Delta P_n = \Delta P_L$ and so the "Laplace force" is given by: $F_p = \Delta P_L \pi D_{ni}^2/4$. Under all these hypotheses, the expression of the maximal weight of a pendant drop at the end of a syringe needle is consistent with Equation (4). By noting the "ideal drop" weight: $M_T g = \gamma \pi D_{ne}$, equation (Eq. 7) provides a correction to Tate's law in the case of a pendant drop generated by a syringe, that is expressed as follows:

$$M_d g = M_T g - \Delta P_L \pi D_{ni}^2/4 \qquad (7)$$

Figure 3b shows the set of experimental results that validates Eq. 7. Figure 9 illustrates more intuitively the meaning of Eq. 7: the maximum weight of the pendant drop is equal to the capillary force exerted at the end of the needle, from which must be subtracted the force coming from the pressure increment applied to the piston and which imposes the value of the

Laplace pressure within the drop. We provide a justification of Eq. 7 by establishing this model under well-identified hypotheses and mathematical developments and it differs from that one suggested by Garandet et al. [29].

Conclusion

This work contributes to the characterization of the weight of pendant drops. It experimentally and mathematically demonstrates the influence of the Laplace pressure on the maximum weight of a pendant drop. The involved physical phenomena in the equilibrium of a pendant drop are well known. However, the writing of the balance of the applied external forces to the pendant drop associated with the rigorous demonstrations of (*i*) the non-influence of the hydrostatic pressure (which appears in the equation of Garandet et al. [29]) and (*ii*) the equality of the overpressure exerted on the piston with the Laplace pressure, lead to an original equation (Eq. 7) providing a correction to the well-known Tate's law. Tate's law [20], based on the theoretical balance of applied external forces to a drop, is usually used to theoretically calculate this weight. Despite numerous criticisms [28-30], to the best of our knowledge, no experimental measurements relating to the validation of Tate's law are reported in the scientific literature. Our work thus constitutes a new basis of reflection associated with experimental data in order to elucidate the factors that determine the weight of a pendant drop.

We have carried out the weight measurement of maximal pendant drops at the end of a syringe needle of different sizes for three liquids of contrasting capillary lengths. The results show a gap with the capillary force alone. These experimental results invalidate Tate's law under the employed conditions. This difference, highlighted with three liquids, is corrected by taking into account the exerted force on the piston in the applied external force balance to a

pendant drop. This force can be related to the Laplace pressure within the drop. A mechanical loading experiment, with imposed capillary force adapted from the works of Li et al. [23] and Neeson et al. [24], is proposed in order to highlight the role of Laplace pressure in the mathematical expression of the maximal weight.

The principle of the mechanical loading with a bead attached to the drop apex, allows to modulate its main curvature and therefore the Laplace pressure. The results show that the mean curvature increases with the mechanical loading according to a master curve which is independent of the liquid characteristics and the needle size. If they are extended to a larger number of liquids, they would provide the basis for a remarkable universality. For each unloaded pendant drop, the curvature is a decreasing function of the drop volume. The relationship between Laplace pressure and the applied force on the piston is mathematically established. An analytical expression of the maximal weight of a pendant drop is deduced. The model, which considers the weight equal to the capillary force, is then revisited and replaced by a new model that explicitly incorporates the Laplace pressure. It is experimentally validated for each tested case.

Our approach can be extended to determine the liquid-solid adhesion work using centrifugal adhesion balance [31, 32]. For this, one needs to replace the piston motion with the increase of the effective gravity performed with centrifugal device. It could be also used to define with high precision the volume that constitutes a pendant drop, especially in the context of downsizing technologies [33]. The better knowledge of the maximum weight of a pendant drop could participate to the improvement of particle coating techniques as used for marbles [4,5]. In the pharmaceutical field, this work could have repercussions on the precision of active drugs formulation distributed as drop (eye drops, perfusion, oral solution in drops…).

Finally, Tate's law is mainly used to characterize the weight of detached drops [19, 21, 27]. The work of Harkins and Brown [21] shows that the ratio of the volume of a detached drop to the volume predicted by Tate's law, varies according to a unique characteristic curve as a function of the capillary radius scaled by the cube root of the detached drop volume. What happens to this relationship if we now consider the real maximum weight of a pendant drop and not the one given by Tate's law? This last point, which constitutes our future work, will bring a new representation of the weight of the drops that fall from a capillary.

CRediT authorship contribution statement

Laure Lecacheux: Conceptualization, Investigation, Methodology, Validation, Visualization, Writing - original draft & editing. Abdelkrim Sadoudi: Conceptualization, Methodology, Validation, Visualization, Writing - original draft. Agnès Duri: Investigation, Validation, Supervision, Writing - review & editing. Véronique Planchot: Formal analysis, Project administration, Resources, review & editing. Thierry Ruiz: Formal analysis, Validation, Methodology, Project administration, Resources, Supervision, Writing - original draft & editing.

Acknowledgments

The authors thank the project DEFI Blé Dur (2016-2022), that has received funding from Programme d'investissement d'avenir (PIA), and the French Région Occitanie for their financial supports.

References

[1] K.J. Obata, T. Motokado, S. Saito, K. Takahashi, A scheme for micro-manipulation based on capillary force, Journal of Fluid Mechanics 49 (2004) 113-121.

[2] P. Lambert, A. Delchambre, A study of capillary forces as a gripping principle, Assembly Automation 25(4) (2005) 275-283.

[3] P. Aussillous, D. Quéré, Liquid marbles, Nature 411 (2001) 924-927.

[4] E. Bormashenko, New insights into liquid marbles, Soft Matter, 8 (2012) 11018.

[5] G. McHale, M.I. Newton, Liquid marbles: topical context within soft matter and recent progress, Soft Matter 11 (2015) 2530.

[6] H.N. Emady, D. Kayrak-Talay, W.C. Schwerin, J.D. Litster, Granule formation mechanisms and morphology from single drop impact on powder beds, Powder Technology 212 (2011) 69-79.

[7] D. Rossetti, X. Pepin, S.J.R. Simons, Rupture energy and wetting behavior of pendular liquid bridges in relation to the spherical agglomeration process, Journal of Colloid and Interface Science 261 (2003) 161-169.

[8] K.P. Hapgood, J.D. Litster, S.R. Biggs, T. Howes, Drop penetration into porous powder beds, Journal of Colloid and Interface Science 253 (2002) 353-366.

[9] B. Bellocq, B. Cuq, T. Ruiz, A. Duri, K. Cronin, D. Ring, Impact of fluidized bed granulation on structure and functional properties of the agglomerates based on the durum wheat semolina, Innovative Food Science and Emerging Technologies 45 (2018) 73-83.

[10] S.M. Iveson, J.D. Litster, K. Hapgood, B.J. Ennis, Nucleation, growth and breakage phenomena in agitated wet granulation processes: a review, Powder Technology 117 (2001) 3-39.

[11] S. Mandato, E. Rondet, G. Delaplace, A. Barkouti, L. Galet, P. Accart, T. Ruiz, B. Cuq, Liquids' atomization with two different nozzles: Modelling of the effects of some processing and formulation conditions by dimensional analysis, Powder Technology 224 (2013) 323-330.

[12] R. Abdelaziz, D. Disci-Zayed, M.K. Hedayati, J.H. Pohls, A.U. Zillohu, B. Erkartal, V.S.K. Chakravadhanula, V. Duppel, L. Kienle, M. Elbahri, Green chemistry and nanofabrication in a levitated Leidenfrost drop, Nature Communications 4 (2013) 2400.

[13] G.A. El-Nagar, O. Delikaya, I. Lauermann, C. Roth, Platinum nanostructure tailoring for fuel cell applications using levitated water droplets as green chemical reactors, ACS Applied Materials & Interfaces 11(25) (2019) 22398-22407.

[14] C. Boissiere, D. Grosso, A. Chaumonnot, L. Nicole, C. Sanchez, Aerosol Route to Functional Nanostructured Inorganic and Hybrid Porous Materials, Advanced Materials 23 (2011) 599-623.

[15] C. Sadek, H. Tabuteau, P. Schuck, Y. Fallourd, N. Pradeau, C. LeFloch-Foueré, R. Jeantet, Shape, shell, and vacuole formation during the drying of a single concentrated whey protein droplet, Langmuir 29 (2013) 15606-15613.

[16] R. Gunde, A. Kumar, S. Lehnert-Batar, R. Mäder, E.J. Windhab, Measurement of the surface and interfacial tension from maximum volume of a pendant drop, Journal of Colloid and Interface Science 244 (2001) 113-122.

[17] A.T. Morita, D.J. Carastan, N.R. Demarquette, Influence of drop volume on surface tension evaluated using the pendant drop method, Colloid and Polymer Science 280 (2002) 857-864.

[18] J.D. Berry, M.J. Neeson, R.R. Dagastine, D.Y.C. Chan, R.F. Tabor, Measurement of surface and interfacial tension using pendant drop tensiometry, Journal of Colloid and Interface Science 454 (2015) 226-237.

[19] O.E. Yildirim, Q. Xu, O.A. Basaran, Analysis of the drop weight method, Physics of Fluids 17 (2005) 062107.

[20] T. Tate, On the magnitude of a drop of liquid formed under different circumstances, Philosophical Magazine 27 (1864) 176-180.

[21] W.D. Harkins, F.E. Brown, The determination of surface tension and the weight of falling drops: The surface tension of water and benzene by the capillary height method, Journal of the American Chemical Society 41 (1919) 499-524.

[22] E. Portuguez, A. Alzina, P. Michaud, M. Oudjedi, A. Smith, Evolution of a Water Pendant Droplet: Effect of Temperature and Relative Humidity, Natural Science 9 (2017) 1-20.

[23] C. Li, J.A. Simmons, M. Moradiafrapoli, J.O. Marston, Direct visualization of particle attachment to a pendant drop, Soft Matter 13 (2017) 1444.

[24] M.J. Neeson, D.Y.C. Chan, R.F. Tabor, Compound pendant drop tensiometry for interfacial tension measurement at zero bond number, Langmuir 30 (2014) 15388-15391.

[25] P.G. de Gennes, F. Brochard-Wyart, D. Quéré, Capillarity and wetting phenomena: drops, bubbles, pearls, waves, Springer-Verlag New York Inc. (2013).

[26] A. Nazari, A.Z. Derakhshi, A. Nazari, B. Firoozabadi, Drop formation from a capillary tube: Comparison of different bulk fluid on Newtonian drops and formation of Newtonian and non-Newtonian drops in air using image processing, International Journal of Heat and Mass Transfer 124 (2018) 912-919.

[27] M.C. Wilkinson, Extended use of, and comments on, the drop-weight (drop-volume) technique for the determination of surface and interfacial tensions, J Journal of Colloid and Interface Science 40 (1972) 14.

569 [28] B-B. Lee, P. Ravindra, E-S. Chan, A critical review: Surface and interfacial tension
570 measurement by the drop weight method, Chemical Engineering Communications
571 195(8) (2008) 889-924.
572 [29] J.-P. Garandet, B. Vinet, P.O. Gros, Considerations on the pendant drop method: a new
573 look at Tate's law and Harkins' correction factor, Journal of Colloid and Interface
574 Science 165(2) (1994) 351-354.
575 [30] A. Kumar, M.R. Gunjan, R. Raj, On the validity of force balance models for predicting
576 gravity-induced detachment of pendant drops and bubbles, Physics of Fluids 32 (2020)
577 101703.
578 [31] R. Tadmor, R. Das, S. Gulec, J. Liu, H.E. N'guessan, M. Shah, P.S. Wasnik, and Sakshi
579 B. Yadav, Solid-Liquid Work of Adhesion, Langmuir 33 (2017) 3594.
580 [32] S. Yadav, S. Gulec, R. Tadmor, I. Lian, A Novel Technique Enables Quantifying the
581 Molecular Interaction of Solvents with Biological Tissues, Scientific Reports 9 (2019)
582 9319.
583 [33] O.A. Basaran, Small-scale free surface flows with breakup: drop formation and
584 emerging applications, AIChE Journal 48(9) (2002) 1842-1848.
585

Figure 1. Scheme of the experimental prototype for pendant drop generation and contouring acquisition of the maximal pendant drop.

Figure 2. Illustration of the curvature radii measurement for a single pendant drop (left) and a loaded pendant drop with a glass bead (right).

Figure 3. (a) Capillary force as a function of the maximal drop weight (Eq. 2) for all experiments, (b) capillary force minored by the "Laplace force" versus maximal drop weight (Eq. 4) for all experiments. The order of the error magnitude is about 10^{-4} mN. The dashed line is a guideline.

Figure 4. Illustration of the drop loading with a glass bead at constant capillary force. The images correspond to pendant water drops just before their detachment and formed with a same needle of diameter (D_{ne} = 1.80 mm) and an increasing load.

Figure 5. Maximal mass of loaded pendant drops as a function of bead mass for Water (circle), Tween 80 (square) and Triacetin (triangle). For each liquid only results, obtained for needles of external diameters equal to 1.26 (empty symbols) and 1.80 mm (blanck symbols), are shown. The dashed lines are a guideline. Full results are available in the Supplementary Materials file.

Figure 6. Variation of the loaded pendant drop curvatures as a function of the solid mass fraction for all experiments: (a) dimensionless curvature radii, (b) dimensionless mean curvature. The dashed lines are a guideline.

Figure 7. Laplace pressure within the maximal pendant drops as a function of the particle mass for (a) Water, (b) Tween 80, (c) Triacetin and different external diameters of the needle (D_{ne} = 0.23, 0.50, 0.80, 1.26 and 1.80 mm). The order of the diameters is respected for each figure. The dashed lines are a guideline.

Figure 8. (a) Variation of the mean curvature as a function of the maximum pendant drop volume (R^2 = 0.9736) for all liquids and needles used (Log-Log representation), (b) Laplace pressure within the maximal pendant drops as a function of its weight.

Figure 9. Scheme of the external forces applied to a maximal pendant drop generated by a syringe.

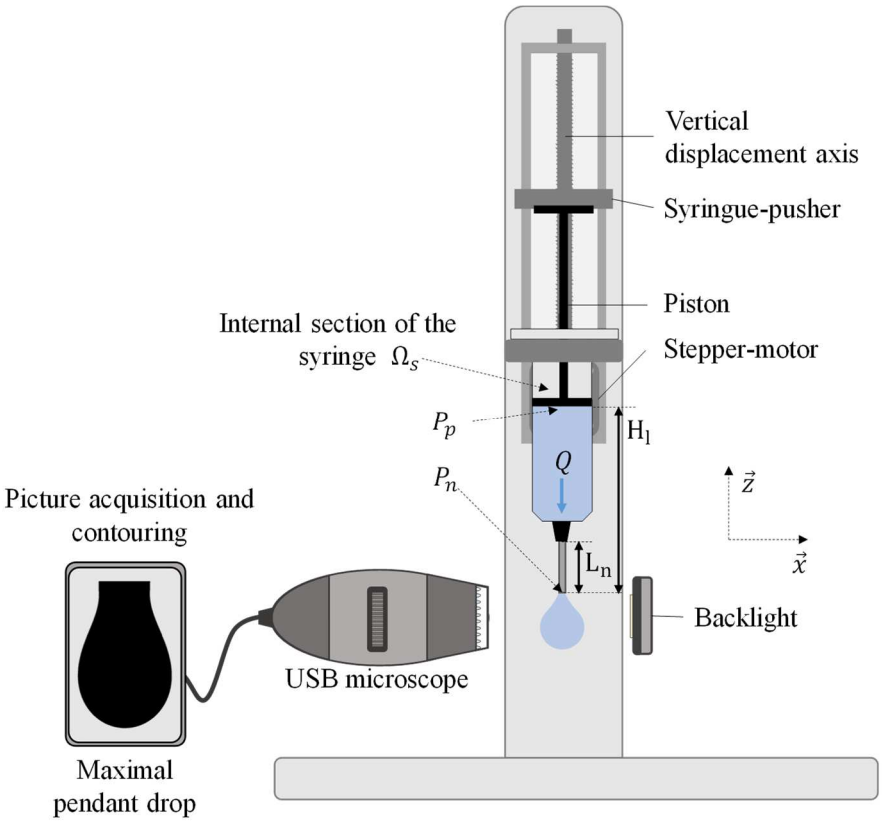

Figure 1. Scheme of the experimental prototype for pendant drop generation and contouring acquisition of the maximal pendant drop.

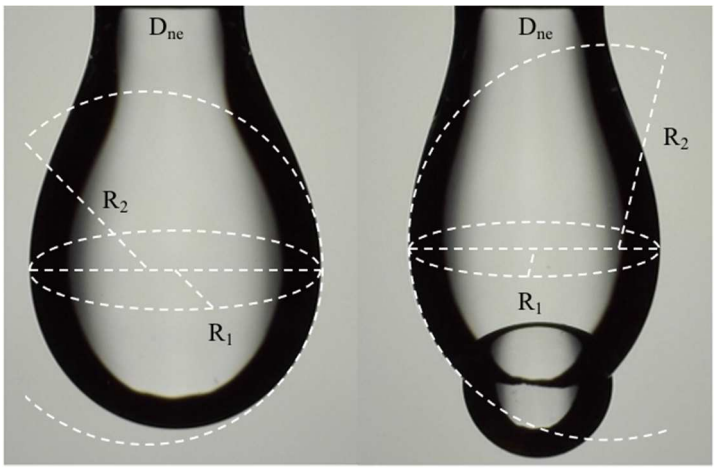

Figure 2. Illustration of the curvature radii measurement for a single pendant drop (left) and a loaded pendant drop with a glass bead (right).

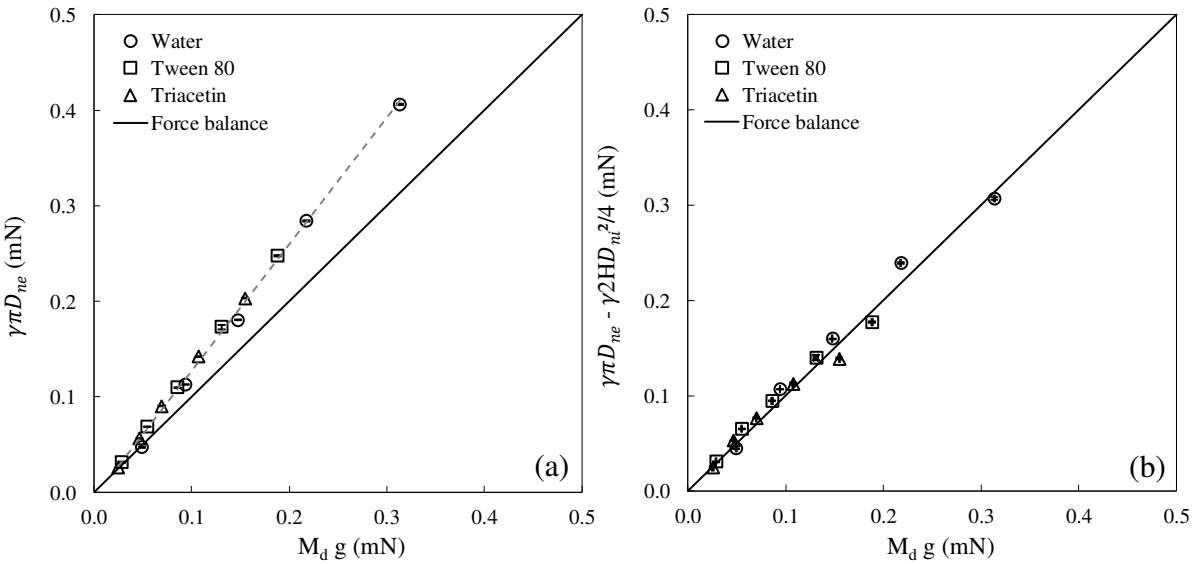

Figure 3. (a) Capillary force as a function of the maximal drop weight (Eq. 2) for all experiments, (b) capillary force minored by the "Laplace force" versus maximal drop weight (Eq. 4) for all experiments. The order of the error magnitude is about 10^{-4} mN. The dashed line is a guideline.

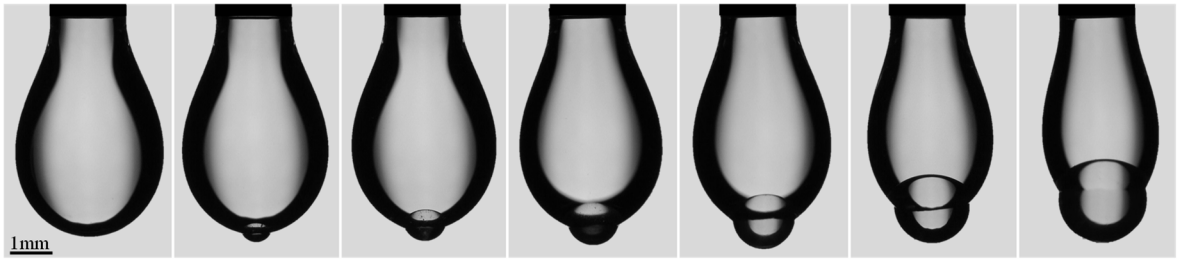

Figure 4. Illustration of the drop loading with a glass bead at constant capillary force. The images correspond to pendant water drops just before their detachment and formed with a same needle of diameter (D_{ne} = 1.80 mm) and an increasing load.

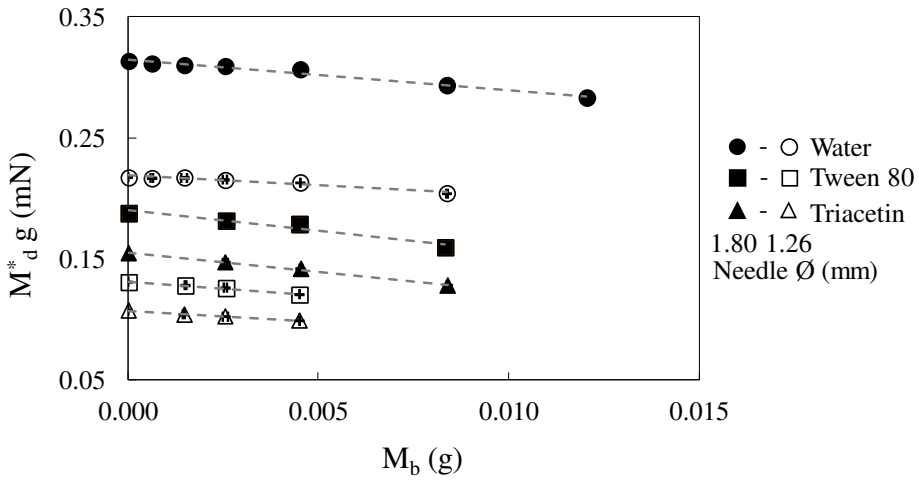

Figure 5. Maximal mass of loaded pendant drops as a function of bead mass for Water (circle), Tween 80 (square) and Triacetin (triangle). For each liquid only results, obtained for needles of external diameters equal to 1.26 (empty symbols) and 1.80 mm (blanck symbols), are shown. The dashed lines are a guideline. Full results are available in the Supplementary Materials file.

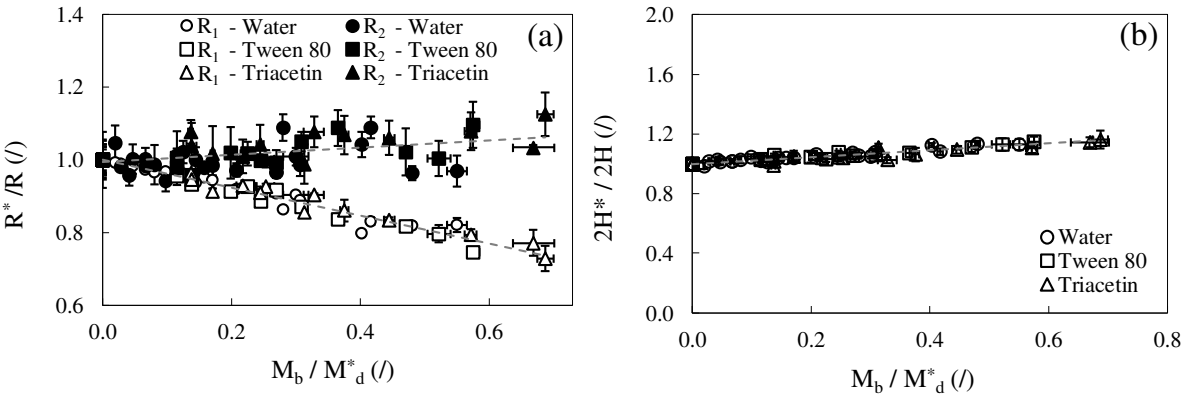

Figure 6. Variation of the loaded pendant drop curvatures as a function of the solid mass fraction for all experiments: (a) dimensionless curvature radii, (b) dimensionless mean curvature. The dashed lines are a guideline.

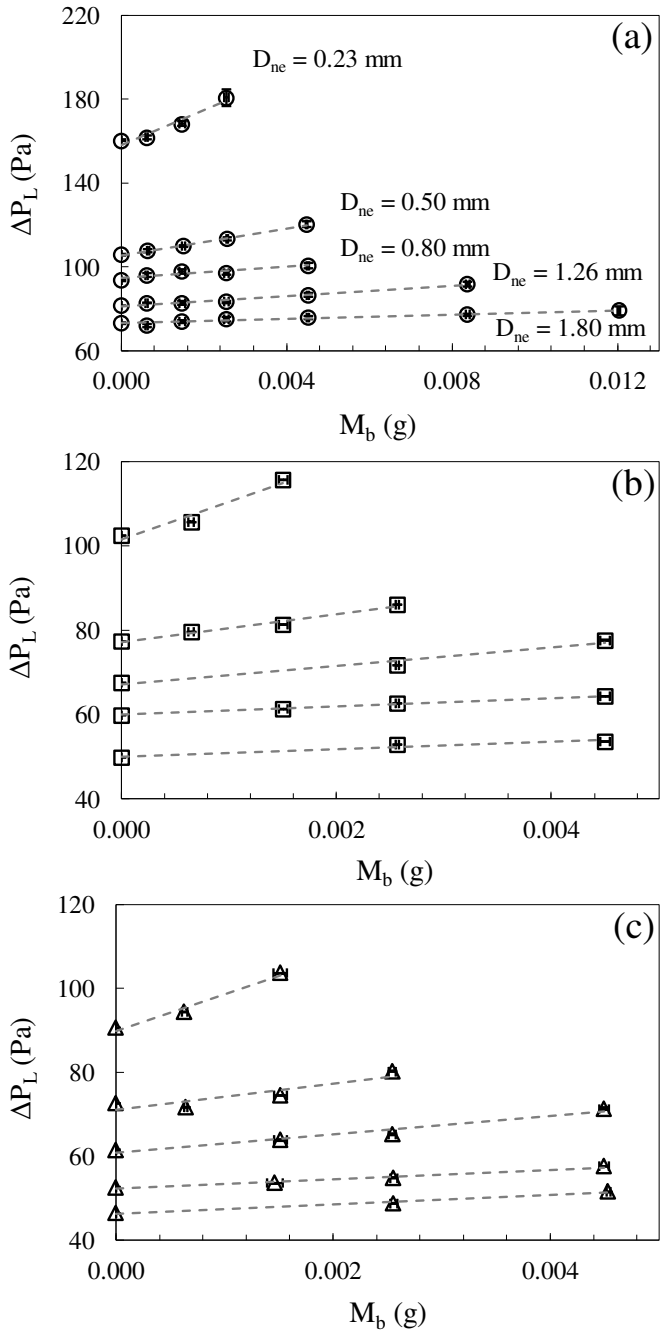

Figure 7. Laplace pressure within the maximal pendant drops as a function of the particle mass for (a) Water, (b) Tween 80, (c) Triacetin and different external diameters of the needle (D_{ne} = 0.23, 0.50, 0.80, 1.26 and 1.80 mm). The order of the diameters is respected for each figure. The dashed lines are a guideline.

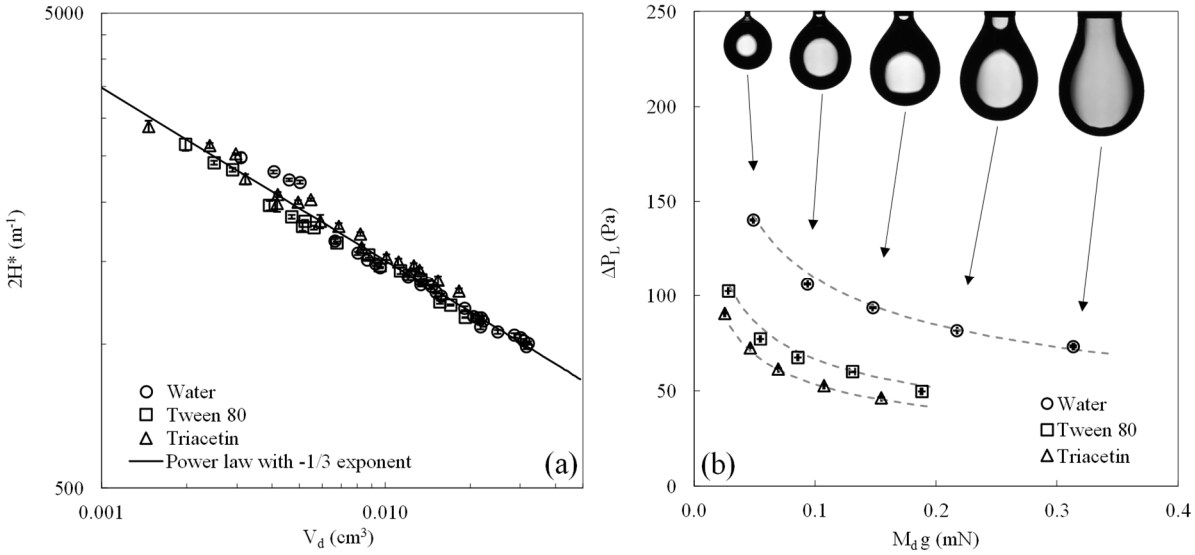

Figure 8. (a) Variation of the mean curvature as a function of the maximum pendant drop volume (R^2 = 0.9736) for all liquids and needles used (Log-Log representation), (b) Laplace pressure within the maximal pendant drops as a function of its weight.

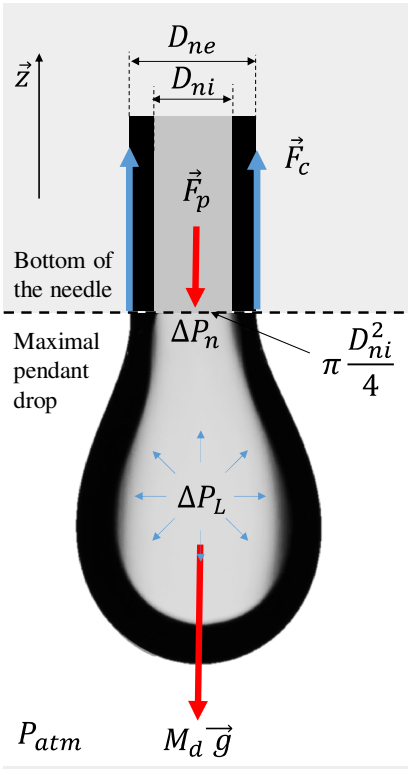

Figure 9. Scheme of the external forces applied to a maximal pendant drop generated by a syringe.

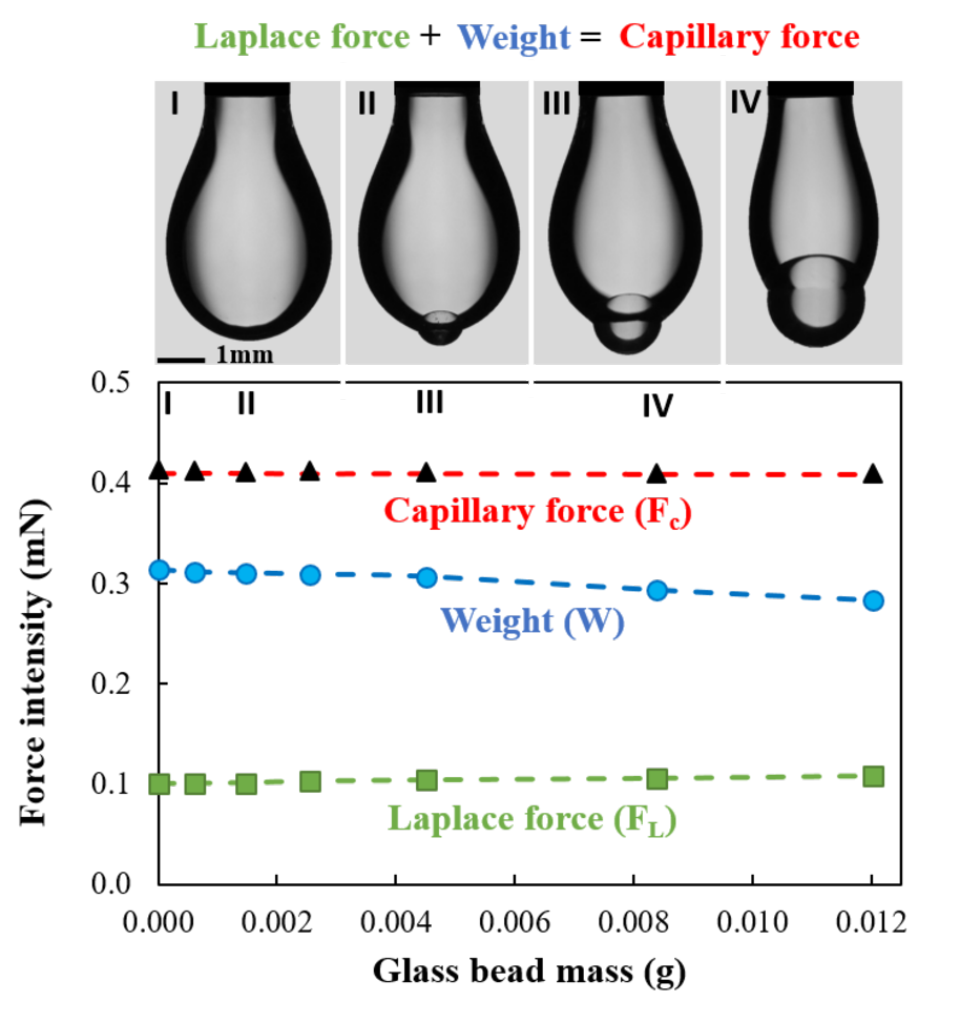
Laplace force + Weight = Capillary force
I
II
III
IV
1mm
0.5
0.4
0.3
0.2
0.1
0.0
Force intensity (mN)
Capillary force (F_C)
Weight (W)
Laplace force (F_L)
0.000
0.002
0.004
0.006
0.008
0.010
0.012
Glass bead mass (g)